Sensors & Actuators: A. Physical 388 (2025) 116491

Contents lists available at ScienceDirect

Sensors and Actuators: A. Physical

journal homepage: www.journals.elsevier.com/sensors-and-actuators-a-physical

A multifunctional platform for the production and customization of polymer-based microneedle devices

Andrea Bocchino [a,*], Carlota Marquez-Grana [a], Om Prakash Singh [a], Eva Melnik [b], Steffen Kurzhals [b], Giorgio C. Mutinati [b], Sion Coulman [c], Christopher Martin [c], Keng Wooi Ng [c], Mariane Massufero Vergilio [c], James Birchall [c], Paul Donovan [d], Paul Galvin [a], Conor O'Mahony [a,*]

[a] Tyndall National Institute, University College Cork, Cork T12 R5CP, Ireland
[b] AIT Austrian Institute of Technology GmbH, Center for Health and Bioresources, Molecular Diagnostics, Giefinggasse, 4, Vienna 1210, Austria
[c] School of Pharmacy and Pharmaceutical Sciences, Cardiff University, Cardiff, UK
[d] Sanmina Corporation, Huntsville, AL, USA

ARTICLE INFO

Keywords:
Microneedles
Moulding
Polymer
Transdermal drug delivery
ECG electrode
Sensors
Medical devices

ABSTRACT

Polymer microneedles (MNs) have significant potential for use in transdermal delivery and diagnostics applications due to their low cost, versatility, and compatibility with medical grade materials and industrial manufacturing processes. These polymers can also have a wide range of different and desirable properties such as biocompatibility, degradability, and flexibility. To facilitate rapid development of these devices, a multifunctional manufacturing process, easily adaptable to a range of different materials and use cases, would be highly beneficial for research and prototyping purposes. With that in mind, we have developed a multifunctional platform that may be used to produce sharp-tipped microneedle arrays with a variety of substrate materials, mechanical characteristics, electrical properties, and diagnostic functionalities. The paper first presents an outline of the platform concept and the double-sided moulding process that lies at its core, followed by a description of the various add-on steps that are used to customise the geometrical, mechanical, electrical, and functional aspects of the arrays. Finally, we illustrate the versatility of the platform with three exemplars, namely a solid, electrochemically active MN sensor for biomarker diagnostics, a fabric-backed, flexible MN electrode for biopotential monitoring, and a biodegradable array for transdermal drug delivery.

1. Introduction

Microneedles are sharp needle-like structures, typically no more than a millimetre in length, and that are capable of painlessly piercing the outermost layer of the epidermis, known as the *stratum corneum* (SC) [1]. The *stratum corneum* typically ranges from 10 μm to 30 μm in thickness [2], and is comprised of densely packed corneocytes embedded in a lipid bilayer matrix [3]. This presents a considerable barrier to the transdermal delivery of drugs and vaccines, prevents the sampling of diagnostic materials, and hinders the passage of electrical and optical signals into and out of the body. Arrays of microneedles may be used to penetrate this barrier and reach the viable epidermis and the uppermost layer of the dermis that lie beneath. Both layers are rich in interstitial fluid-borne biomarkers and immune-responsive cells, and lie close to the capillary network, making them an ideal target for bloodless diagnostics and for the transdermal delivery of drugs and vaccines. Moreover, because of their short length, MNs do not strike the nerve endings nor the capillary vessels that lie deeper in the skin; their use is therefore perceived as painless and bloodless by the user. MN arrays are easy to both apply and dispose of, and reduce any risk of needle-phobia that could lead to patient non-adherence [4,5]. Due to these properties, MNs have been widely investigated for many applications including delivery

* Corresponding authors.
E-mail addresses: andrea.bocchino@tyndall.ie (A. Bocchino), carlota.marquez@tyndall.ie (C. Marquez-Grana), omprakash.singh@plymouth.ac.uk (O.P. Singh), eva.melnik@ait.ac.at (E. Melnik), steffen.kurzhals@ait.ac.at (S. Kurzhals), giorgio.mutinati@ait.ac.at (G.C. Mutinati), coulmansa@cardiff.ac.uk (S. Coulman), christopher.martin@rpharms.com (C. Martin), keng.ng@newcastle.ac.uk (K.W. Ng), M262908@dac.unicamp.br (M. Massufero Vergilio), birchalljc@cardiff.ac.uk (J. Birchall), paul.donovan@sanmina.com (P. Donovan), paul.galvin@tyndall.ie (P. Galvin), conor.omahony@tyndall.ie (C. O'Mahony).

https://doi.org/10.1016/j.sna.2025.116491
Received 4 March 2025; Accepted 17 March 2025
Available online 21 March 2025

of drugs [6,7] and vaccines [8], biomarker diagnostics [9], detection of biopotentials such as ECG, EEG and EMG signals [10–12], enhancement of optical transmission through skin [13], and electroporation/iontophoresis [14].

Considering the numerous different applications MNs can be used for, they have been fabricated using a wide variety of materials and techniques. Typical examples include silicon, metals, resins, polymers, silk, ceramics and sugars produced by techniques such as etching, laser cutting, electro-polishing, 3D printing and micromoulding [15,16].

Because of their low cost, medical grade and compatibility with high-volume manufacturing techniques such as injection moulding, polymer materials have the potential to reduce the cost of the MN devices together with the complexity of the production process [17,18]. Moreover, polymers exhibit a large variety of properties that are appealing for MNs production. Biocompatible, degradable, swellable, flexible and rigid MNs may all be fabricated by simply choosing the appropriate polymer [19]. Examples of these needles are shown in Table 1.

From this brief summary, it is evident that polymers have been widely used for many different microneedle applications, and all devices and materials referred to in Table 1 are available in grades that comply with biocompatibility testing standards such as ISO 10993–1 and USP Class VI. To facilitate rapid development of these devices, a multifunctional manufacturing process, easily adaptable to a range of different materials and use cases, would be highly beneficial for research and prototyping purposes. With that in mind, we have previously developed a wafer-level micromoulding process for the manufacture of sharp-tipped microneedle arrays for biosensing applications [38]. In this work, we extend that process to develop a multifunctional platform that may be used to produce arrays with a variety of substrate materials, mechanical characteristics, electrical properties, and diagnostic functionalities. The platform represents a significant evolution of the original process, not only because it allows the use of degradable and swellable polymers, but also because it can accommodate the merging of several materials within the same device. Moreover, the use of a modular vacuum table, shown in Section 2.1, increases the production throughput, thereby scaling up the process from the original work and enabling batch production capabilities.

An outline of the platform concept and the double-sided moulding process that lies at its core is provided in Section 2, followed by a description of the various add-ons that are used to customise the geometrical, mechanical, electrical, and functional aspects of the arrays. Finally, we illustrate adaptability of the platform by showing its application in three different applications, namely biomarker diagnostics, biopotential monitoring and transdermal delivery.

2. Platform design

The aim of this work is to develop a multifunctional process that could easily be used to quickly prototype MN arrays for different applications. To arrive at such a one-fits-all platform, a core technique to fabricate a wide range of array types is an essential element of the entire concept. The foundation of our platform is a double-sided, vacuum casting micromoulding process, which has been adapted to the batch fabrication of polymeric wafer substrates.

Starting from this core, different ‘building blocks’ have been developed and may be used as required to fully customize the MN arrays. Firstly, the mould templates are tailored to the intended use case in terms of array size and shape, electrical vias, needle height, and surface topology. Then, based on the required properties of the final application, the structural polymers are selected. These different materials will provide the necessary biomechanical (such as flexibility), or functional (such as biocompatibility, degradability or optical) properties. While the process is generally implemented using a single material to form monolithic needles, in some cases the substrate and microneedles may require different properties and therefore two separate materials will be used.

Table 1
Review of different polymer MNs arrays.

Materials	Application	Production Process	Features	Ref.
OrmoComp	pH monitoring	UV-cured Polydimethylsiloxane (PDMS) mould, Si master	Metallized (sputter), multi-electrodes	[20]
1201AB−3 hard epoxy, 607AB−5 soft substrate	ECG, EMG recording	Moulding in PDMS, acrylic machined master	Metallized, flexible arrays	[21]
Unspecified “Class I biocompatible resin”	Anticancer therapy	Stereolithography	Biocompatible, inkjet coating	[22]
Polylactic acid (PLA)	Drug delivery	FDM 3D printing and etching sharpening	Coated, biodegradable, loaded	[23]
Polyimide	ECG, EMG, EOG recording	Moulding in PDMS, steel MNs on printed circuit board (PCB) master	Metallized (sputter), flexible arrays	[24]
Curable magnetorheological fluid (CMRF), epoxy-based	Drug delivery	Magnetorheological drawing lithography (MRDL)	Metallized, flexible, micro-patterned arrays	[25]
Polycarbonate	Lactate detection	Injection moulding	Metallized, functionalised sensors	[26]
CMRF	ECG, EMG, EEG recording	MRDL	Flexible, metallized (sputter), laser-direct writing (LDW) patterning	[27]
Methacrylated hyaluronic acid (MeHA)	Interstitial fluid (ISF) extraction	Moulding in PDMS, steel master	Swellable, loaded, MNS for sensor integration	[28]
Polyethylene glycol (PEG)	Drug delivery	Centrifuge assisted moulding	Swellable, controllable cross-linking	[29]
SU−8 50 photoresist	Glucose monitoring	UV-curing in spinning PMDS mould, electrically discharged machined (EDM) aluminium master	Metallized (conformal sputter), functionalized	[30]
Layered Polyvinylpyrrolidone (PVP) and Poly lactic-co-glycolic acid (PLGA)	Bi-phasic drug delivery	Spray deposition in PDMS mould	Biodegradable, implantable, drug loaded matrix	[31]
PLA and PLGA	Contraceptive delivery	Centrifuge assisted moulding	Biodegradable, implantable, drug loaded matrix, bubbles	[32]
PVP	Cosmetic delivery	UV polymerization in laser written PDMS mould	Biodegradable, drug loaded matrix	[33]
Polymethyl methacrylate (PMMA)	Drug delivery	Moulding in sacrificial PVA, lithography formed electroplated PMMA master	Hollow, formed from a sacrificial intermediate mould	[34]
Polycarbonate	Antibiotic monitoring	Injection moulding	Functionalised, metallized (e-beam), passivated	[35]
SU−8 photoresist	Biopotential measurement	Moulding from PDMS, parylene-coated PDMS master	Biocompatible, passivated, metallized (vapour-deposition)	[36]
Silk fibroin	Wound healing, monitoring/sensing	Moulding from PDMS, laser engraved mould	Origami structure, patterned microfluidic, biocompatible	[37]
Polyethylene glycol diacrylate-sodium alginate and dopamine-gelatin	Drug delivery	Moulding	Nature-inspired structures for enhanced adhesion, biocompatible, swellable	[37]

If electrical functions are required, metal deposition techniques such as evaporation or sputtering may be used to define electrodes, tracks, interconnect, and functional areas. These layers typically use vias created during the initial moulding stage to establish front to rear connection without the need for a separate via formation step.

For many applications, particularly in biosensing, it is desirable to ensure that only the surfaces of the microneedles themselves are in contact with the skin [39]. Therefore, passivation layers may also be added to the platform to block unwanted interference arising from the contact between the array substrate and the skin.

Lastly, a coating step is often required in both drug delivery and diagnostics [40]. For transdermal delivery of drugs and vaccines, arrays may be coated using a range of spraying, dipping, dropping and immersion processes with therapeutic agents that subsequently dissolve in the skin [41]. In electrochemical diagnostics, needle tips may be functionalised with electroactive analytes, such as enzymes or antibodies, that react with a specific target [42].

A summary of this multifunctional process is represented in Fig. 1.

In the next section, the core production process will be presented, followed by a description of the additional steps that can be used to customise the platform.

2.1. Micromoulding process

The micromoulding process, an early version of which was described in a previous publication [38], used two flexible, PDMS moulds to form a polymeric MN wafer. The front mould was the negative copy of a silicon master template on which 500 μm tall MNs were etched, while the rear mould was formed from a milled glass template and used to define the outline of circular, detachable arrays. This fabrication approach already simplified and sped up the manufacturing of the arrays, pre-forming them on the wafer and enabling through-wafer electrical connectivity without the need for additional wafer dicing and interconnect steps.

In this paper, the technique has been expanded to accommodate the use and combination of different materials and master templates, Fig. 2.

Similarly to the original process, two moulds are made by mixing PDMS (Sylgard 184 Silicon Elastomer Kit, Dow Chemical Company, MI, USA) according to the manufacturer's instructions and pouring it over the front and rear master templates, which may be formed from any desirable process or material. The front template defines needle geometry, pitch, and surface topology, while the rear template defines array shape and size, through-wafer vias, and, when needed (see Section 2.3), marks for mask alignment. After cooling, the PDMS moulds are removed from the templates (Fig. 2A and Fig. 2B). The polymer of choice is then poured on the front mould which is placed on a customised vacuum table (VT), shown in Fig. 3.

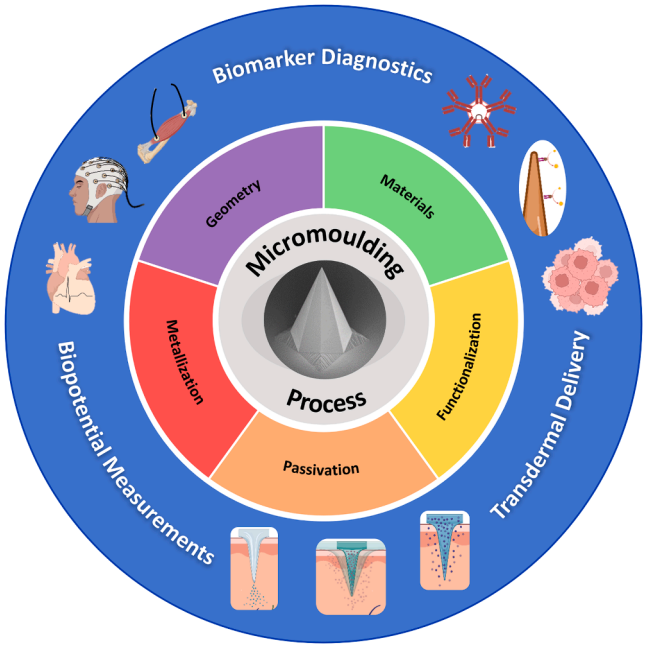

Fig. 1. Schematic representation of the platform design. In the centre: SEM picture of a 500 μm tall microneedle. Adapted from image created with BioRender.com.

Since PDMS is permeable to gases [43], application of negative pressure to the rear of the PDMS layer can aid in drawing the material into the mould, thereby aiding in filling of the cavity tips and improving microneedle sharpness. In this case, the VT is connected to a negative pressure source of approximately 1 bar, which is usually maintained for a minimum of 20 minutes. The VT was designed using a modular format to easily scale up the production throughput at laboratory level, together with enabling parallel testing of different material formulations or production conditions. This is an improvement over the previously used process, which could handle the preparation of a single wafer per iteration [38]. At present, the production of a batch of up to 4 × 100 mm diameter substrates is possible, although this could be extended as required by connecting additional stations to the VT. If needed, less than four wafers may be processed simply closing the valves of the unused stations. The production of a batch of four wafers can be used as a practical example to highlight the advantages of the modular VT over the previous process. In the previous single-wafer production, the polymer of choice was prepared, sandwiched in between the PDMS moulds, positioned on the VT, and then cured. This process was carried out one wafer at the time. Excluding curing, each wafer took a total of 25 minutes to mould: 5 minutes preparation time, and a further minimum time of 20 minutes on the VT. When using the modular VT, a proportionately larger quantity of polymer was prepared and subsequently divided over the four different front moulds. Similarly, by having 4 vacuuming stations, all wafers were simultaneously exposed to low pressure for 20 minutes. Therefore, only 25–30 minutes were required for the production of the four-wafer batch, resulting in significant time savings over the singular approach.

If a monolithic device is required, the rear mould may be placed over the uncured polymer at this point. A metallic cylinder, weighting 500 g, was applied to the rear of the mould-polymer-mould stack aids in ensuring that the two moulds come into intimate contact over the entire area. The arrays are finally hardened by either curing or drying the polymer as required before removal of the moulds.

If a bilayer construction is preferred, excess material is removed with a spatula (Fig. 2C) whilst the mould is on the vacuum table, as the negative pressure helps to retain polymer within the MN pockets during the removal process. The needles are then cured or dried before the application of the substrate material (Fig. 2E). This deposition and removal step can be repeated several times to fabricate needles from a variety of different materials on the same array. In this case, a temporary layer, such as Kapton tape, is applied to either block off selected areas of the front mould (Fig. 2C) or to protect the previously formed MNs while casting and removing the second polymer (Fig. 2D). Depending on material requirements, the needles are either UV/heat cured or dried at room temperature, and the substrate layer is then applied (Fig. 2E). If needed, materials such as pre-formed films, components or fabrics may be used as a substrate instead of a mouldable polymer. In this case, these materials are pressed against the polymer needles before curing. A video, included as supporting information, provides a visual representation of the process, showing the different steps in detail.

2.2. Geometry

It is essential that the platform allows full control over the geometrical design of the moulded MNs. This may be done in two ways: by changing the master templates used in the core process and, if any electrical functionality is needed, by defining appropriate masks for the

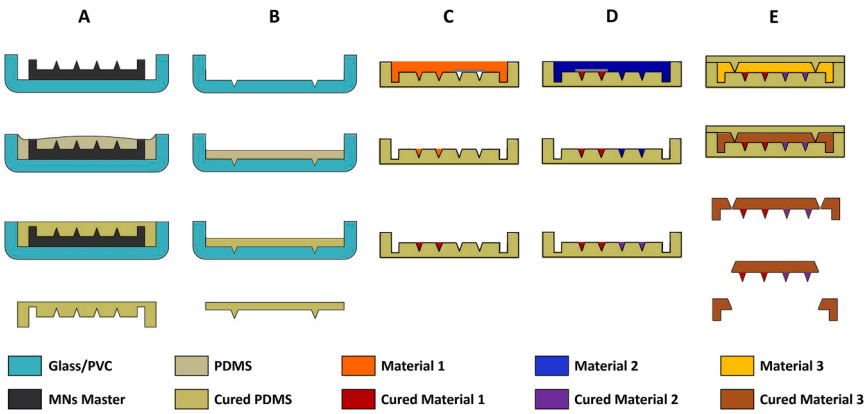

Fig. 2. Schematic of the core production process used to form MN arrays. In this example, microneedles are moulded from two different materials on a substrate of a third material. After preparing the front and rear moulds (A and B, respectively), the MNs (C and D) and the substrate (E) are formed using the desired materials. The shape of the arrays is dictated by the rear mould design while the materials are selected based on the desired properties of the device. To populate the array with different type of needles, tape is used to selectively protect areas of the front mould (C and D) as needed.

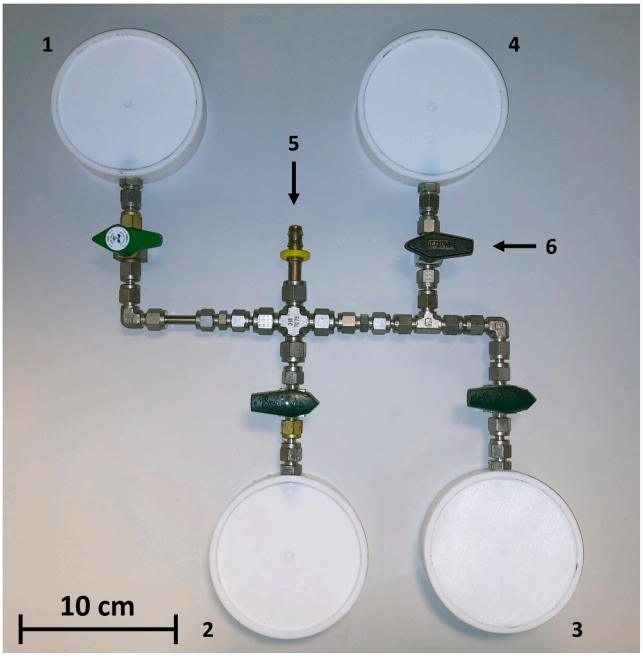

Fig. 3. Modular vacuum table equipped with four polytetrafluoroethylene (PTFE) vacuuming stations (numbered 1–4). A vacuum can be applied to the entire table via the general inlet (5). Each station can be individually disconnected from the vacuum simply closing the corresponding valve (6).

metallization (see Section 2.3).

The front master template defines the shape, pitch, and height of the MNs. In addition to conventional microfabrication techniques such as silicon etching, the development of additive manufacturing technologies has enabled the precise fabrication of microscopic structures. Several groups have used this approach to print MNs that are either too expensive or too difficult to produce using tradition silicon-based processes [6,44–46]. It is of paramount importance that the core moulding process is capable of precisely replicating these complex structures. Therefore, a total of four different designs have been used to fully evaluate the moulding capabilities of the fabrication procedure: 1) Tyndall's silicon MNs, wet-etched from a 100 mm diameter wafer to form 500 μm tall octagonal pyramids with a pitch of 1750 μm [47]; 2) 3D printed conical MNs also with a height of 500 μm and a pitch of 1750 μm, but with a 60 μm reservoir designed close to the tip. These arrays were produced by Upnano (Vienna, Austria) using an NanoOne printer with a 10x objective and UpPhoto resin; 3) 3D printed needles slanted at an angle of 60° to the horizontal, at a pitch of 615 μm between needles, 1050 μm between MN rows, and designed with 4 different heights (165, 345, 555 and 775 μm respectively). These arrays were produced by Boston Micro Fabrication (BMF, Maynard, USA), using a 2 μm resolution S130 printer and HTL-Y resin; 4) microneedles designed by Johannes Kepler University Linz (JKU) in the shape of 210 μm tall square pyramids incorporating a surface pattern of biomimetic features as small as 2 μm, intended to aid the transport of liquids over the needle surface for coating purposes. A 515 nm laser with a 290 fs pulse and 1 MHz repetition rate was used to produce the patterned MNs in OrmoComp resist [46].

All designs were glued to a support that was printed using a Formlab 3 + printer (Solid Print3D Ltd, UK) and white resin (F2GPWH04 from Solid Print3D Ltd, UK), and attached inside a petri dish to form the master template. A medical grade epoxy (Epotek 353ND from Epoxy Technology Europe GmbH, Augsburg, Germany) was used to mould the needles. SEM pictures of the results can be seen in Fig. 4. The moulding process copied all features of the masters with a high degree of fidelity, proving its usability with different types of templates.

Fig. 5 shows examples of both a front and a rear mould, together with close ups of some of the key features. While any suitable process or material can be used to form the rear master template, in this example the desired profile is milled inside a polyvinyl chloride (PVC) Petri dish. To facilitate front-to-rear electrical connection using holes or vias moulded through the polymer, 45°-angled conical cavities were milled on the rear master, Fig. 5C. To help achieve optimal via formation on the wafer, the resulting PDMS cone should be designed to be 25 % higher than the rest of the profile; the PDMS compresses slightly once the two moulds are brought into contact, ensuring intimate contact between the surfaces, and alleviating the risk of unwanted polymer blocking the via channel. Electrical links between the faces of the arrays can then be achieved by simply metallizing both sides of the substrate and vias. Similarly, additional features, such as alignment marks (Fig. 5D), can be milled into the master if required.

The rear master also defines the shape of the arrays using ridge-like features, and short gaps in these ridges, Fig. 5E and Fig. 5F, are used to form tabs that hold the moulded array to the carrier frame of the wafer. Light finger pressure or pick-and-place tools may subsequently be used to detach the arrays from the frame.

2.3. Metallization

A metallization step is necessary to make electrically functional MNs for use in applications such as biosensing, biopotential monitoring,

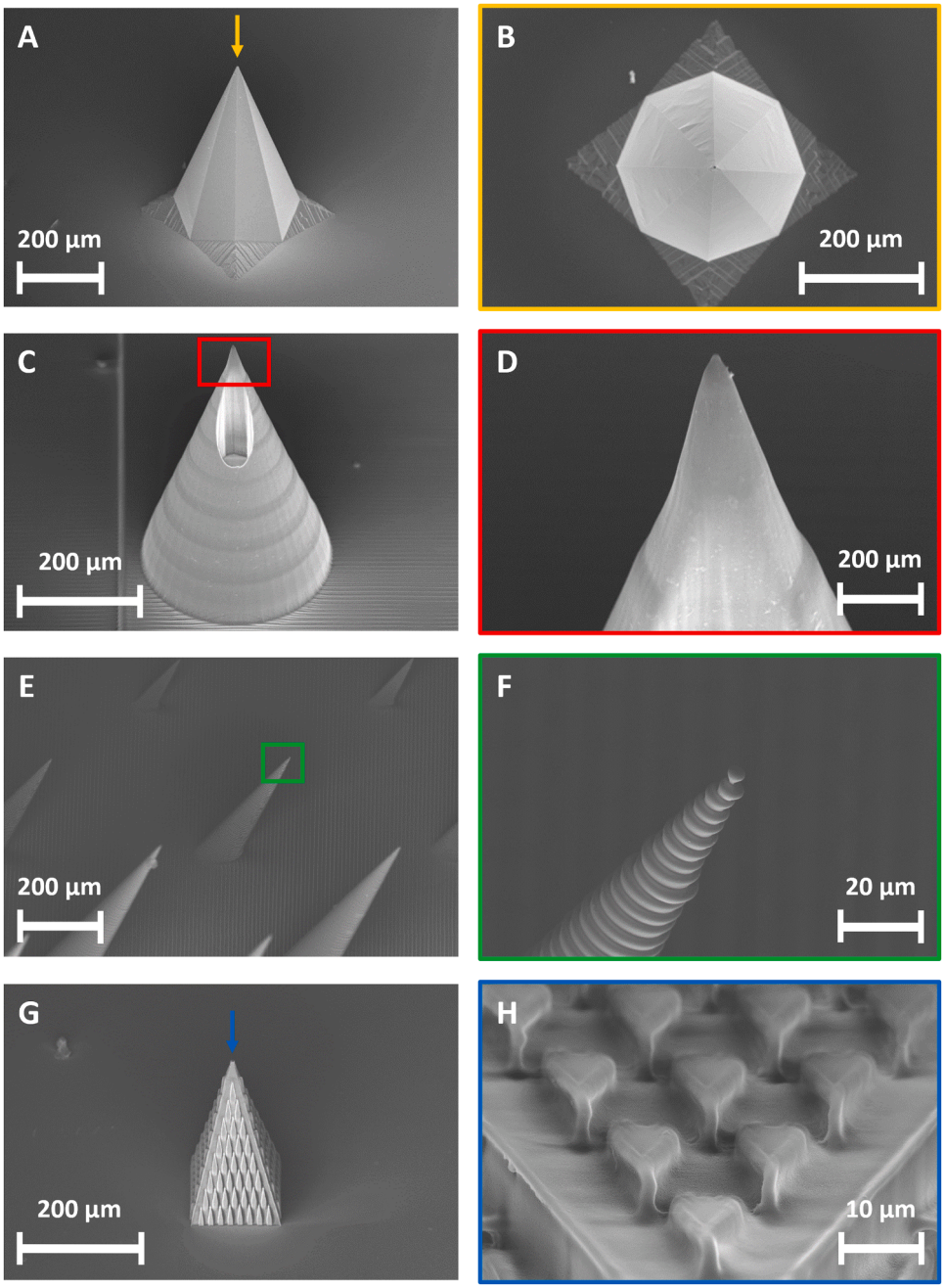

Fig. 4. Different type of moulded MNs: Tyndall's MNs (front, A, and top view, B), Upnano-printed MNs (front side, C, and magnification of the tip, D), BMF-printed MNs (front side, E, and magnification of a tip, F) and JKU's MNs (front side, G, and top magnified view of the pattern, H).

iontophoresis, or electroporation. Different metals can be used for different purposes. For example, gold (Au), platinum (Pt) and silver (Ag) are commonly used for sensor development, while titanium (Ti) and chrome (Cr) are usually implemented as adhesion layers to strengthen the bond between other metals and the substrate. Two main techniques can be used to deposit a thin metallic layer over the arrays: chemical vapour deposition (CVD) and physical vapour deposition (PVD).

CVD processes chemically drive a reaction on a substrate. There are two main CVD technologies: low-pressure CVD (LPCVD) and plasma-enhanced CVD (PECVD). The deposition is thermally induced, and therefore, it heats up the substrate itself. LPCVD uses temperatures higher than 600 °C to slowly grow homogeneous layers on the material. On the other hand, PECVD operates at lower temperature, typically between 200 °C and 400 °C, but the film growth is faster and therefore less precise [48]. Our platform uses polymers to form the MNs. Polymers generally have low glass transition temperatures and melting points. Therefore, CVD processes are not suitable as main metallization technique.

PVD processes aim at freeing material from a metal source and transferring it directly on the substrate. Typical PVD techniques include thermal evaporation [48,49], electron beam (e-beam) evaporation [49] and sputtering [48]. Thermal evaporation heats up the source material and generates a vapour flux from the source to the substrate. Since this method is generally used for low melting point metals and it is not ideal for the fabrication of thin layers [50], it is not a suitable option for use with this platform. E-beam uses high energy electron beams to vaporize even high-melting point metals [49], while sputtering bombards the source with particles to free atoms or molecules that can condense on the substrate [48]. E-beam evaporation and sputtering are both viable options for polymer MNs metallization and this is clearly visible from

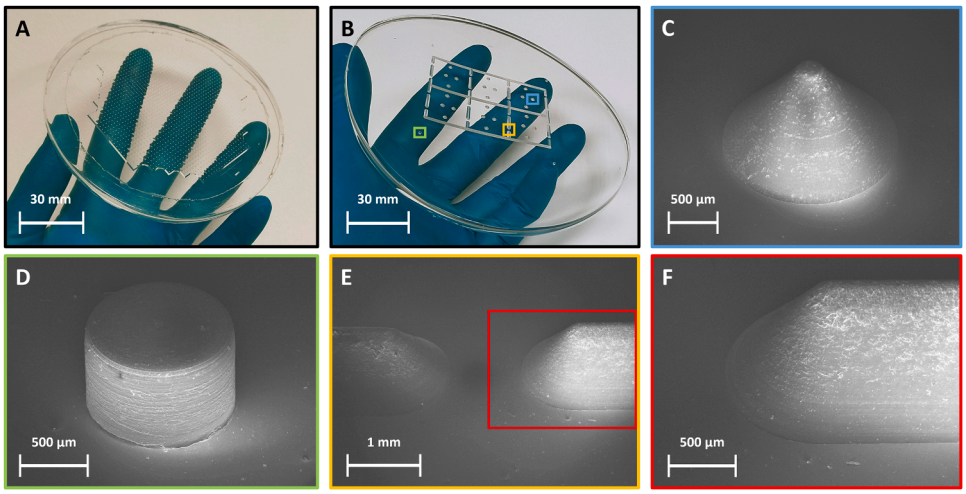

Fig. 5. PDMS moulds produced from the front (A) and the rear (B) master. SEM pictures of the distinctive features present on the rear mould: cones for front-to-rear via formation (C); cylindrical alignment marks (D); ridges with gaps (E, F) to define the shape of the array and the tabs that hold the arrays to the wafer frame.

Table 1.

Finally, metals can be deposited using electroplating. Electroplating is an electrochemical deposition technique that produces a metal coating on an electrically conductive material [51]. However, polymers are generally not electrically conductive and therefore would require a preliminary metal coating in order to be electroplated [50]. Therefore, this method will not be considered as a primary metallisation step in this work.

Both e-beam and sputtering were investigated for MNs metallization. The systems used in this study were a Quorum Q300TD (Quorum, UK) sputterer and a Temescal EUFC4900 (Ferrotec, USA) e-beam evaporator. Both techniques can be used to completely cover the substrates with a metal layer. However, when a specific metallic pattern has to be deposited on the MN arrays, a mask must be used. To avoid damaging

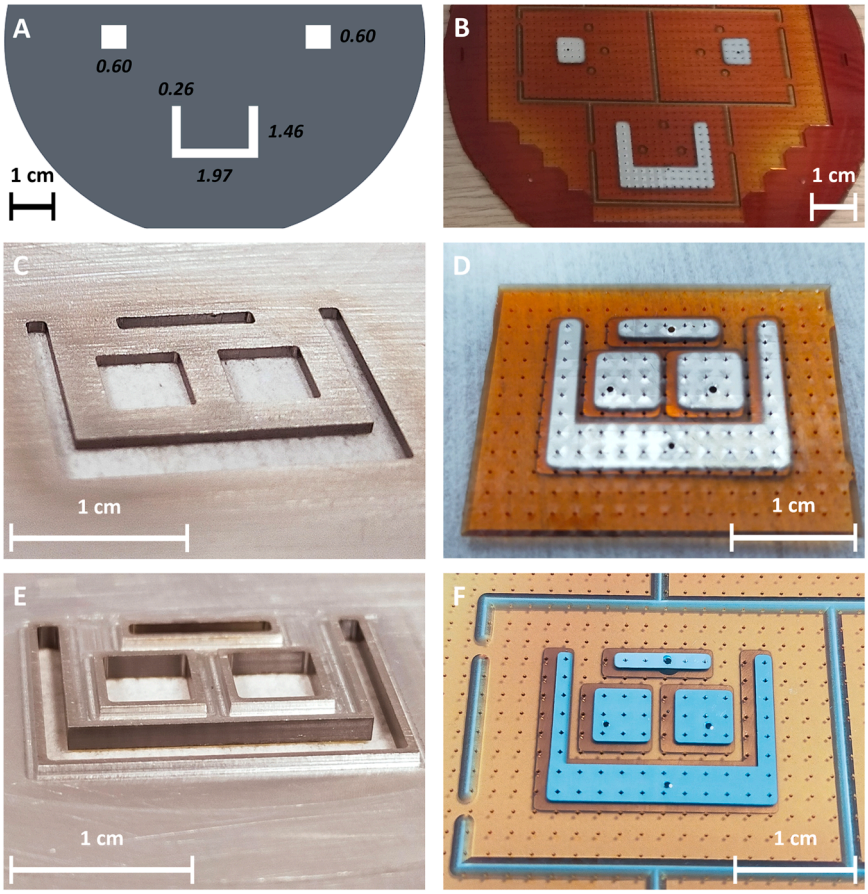

Fig. 6. (A, B) Initial test mask design (features dimensioned in cm), together with resulting sputtered metal pattern – note the blurred patterns due to spreading of the metal under the mask. (C, D) An undersized metal mask with associated metal pattern – some blurring is still visible although the dimension accuracy has improved. (E, F) Undersized mask incorporating protruding walls intended to prevent unwanted metal spreading, along with resultant biosensor electrode pattern.

the needles, no mask can be place in contact with the tips. Therefore, any metallization must be carried out using the mask in close proximity with the substrate, potentially exposing the wafer to deposition of the metal beyond the desired masked area and leading to a spreading or blurring of the intended feature [52]. This effect is similar to photolithographic diffraction when exposing in proximity. Polymer MN wafers were produced and metallised with patterned aluminium masks to test the severity of this effect with both techniques. Tyndall's 500 μm tall silicon MN wafers were used as a front master template. The rear master template was formed as described in Section 2.2 and was designed to divide the wafer into four rectangular arrays, each provided with four through-vias to enable multiple front-to-rear electrical connections. The masks were formed by milling test patterns, Fig. 6 A, in 100 mm aluminium disks. The original thickness of the disks was 1.1 mm, into which a 100 μm deep central recess was milled to avoid physical contact between the mask and the tips of the MNs. Therefore, when the mask is pressed against the wafer, it is 100 μm and 600 μm away from the tip of the needles and from the substrate, respectively. Two masks were used to metallise each wafer: one positioned in hard contact with the rear of the substrate while the second, exploiting the recess, was positioned over the front side of the MNs. The masks were aligned with the wafer and affixed to it using Kapton tape (Farnell, Ireland). Ti and Pt were deposited as test materials, in thicknesses of 20 nm and 100 nm respectively. No significant difference between the mask designs and deposited patterns was observed either for the masks in hard contact with the rear of the wafer, or for the e-beam proximity-masked deposition on the front. However, as shown in Fig. 6B, sputtered patterns showed a high degree of spreading, leading to a significant loss of precision.

To quantify this loss, the resulting test pattern dimensions were measured with a Vernier calliper and compared with the designed mask dimensions. The deposited pattern had dimensions that were (0.8 ± 0.2) mm greater than those of the mask, i.e. a metal spreading of 0.4 mm on each edge was observed. This is an issue both because of the lack of precision and because of the potential for unwanted electrical connections between interconnects or electrodes. The length or the direction of the feature did not seem to affect the magnitude of the spreading. Therefore, smaller features will be proportionally less precise than bigger ones.

To solve this problem, the mask can be undersized to compensate for the metal spreading. Based on the previous analysis, a new metal mask was designed, reducing the size of each dimension by 1 mm. This new mask was intended to form a biosensor on the MN arrays, incorporating one rectangular reference electrode (RE), two square working electrodes (WE) and a counter electrode (CE) wrapping around the other three. The fabricated mask and the resulting sputtered metallization patterns can be seen in Fig. 6 C and Fig. 6D respectively.

The smaller openings produced electrode dimensions closer to the target designs; the metallised pattern had dimensions (0.3 ± 0.1) mm smaller than intended. Further iterations are likely to reduce this remaining error further. The sensors were then tested using a multimeter both to check the quality of the front-to-rear electrical path and to assess unwanted inter-electrode connections. The resistance of the front-to-rear connection established by the through via was consistently below 25 Ω. However, undesired inter-electrode connections, with electrical resistances ranging from tens of kΩ to a few MΩ, were observed. Although this may not be a problem when electrodes are distant from each other, it could become an issue when the form factor of a sensor has to be minimised and the electrodes are, like in this case, closely packed. This effect is also assumed to be due to spreading of the metal in the gap underneath the mask and was not observed when e-beam evaporation was used as a deposition technique.

As an additional measure to physically prevent any undesired metal spreading, pattern blurring and unwanted electrical connections during the sputtering process, wall-like features were incorporated at the edges of the mask openings. These protrusions must come into hard contact with the substrate in between the MNs without touching the needles themselves. An iterative process for sizing the walls has led to walled features of 600 μm deep, accounting for both the recess and the needle height, and a thickness not higher than half the base-to-base distance between MNs. Using a walled mask (Fig. 6E), the resulting sensor (Fig. 6 F) showed no inter-electrode electrical connections.

In summary, e-beam is the preferred metallization technique due to its high precision and lack of metal spreading underneath the mask. Sputtering may also be used, although the high level of metal spreading may lead to dimensional inaccuracies and limit its use for densely packed features. The implementation of wall-like structures on the masks may be used to prevent this problem but increases the complexity and, consequentially, the cost of the masks.

2.4. Materials

Although the platform may be used to simply form monolithic wafers, different substrate and/or microneedle materials may be combined as required. The MNs themselves must be made with a mouldable material and be robust enough to pierce the skin without breaking. For the purposes of this work, a polymer was considered mouldable if its viscosity was not more than approximately 5000 cPs at room temperature. Additional properties that may be of interest for the MNs are biocompatibility, biodegradability, and absorption capabilities. To date, a range of polymers have successfully been used at the core of the platform, including a medical grade epoxy (Epotek 353ND from Epoxy Technology Europe Ltd, UK) [53], a UV curable medical grade photopolymer (NOA 68 from Edmund Optics, UK) [54], several degradable polymers including polyvinylpyrrolidone (PVP), polyvinyl alcohol (PVA), PVP-PVA mixtures, polycaprolactone (PCL), poly(lactic-co-glycolic acid) (PLGA), PCL/PLGA mixtures, sugars including trehalose anhydrous (TRA) and sucrose (SUC), and swellable hydrogels including Gantrez S-97 and Gantrez AN-139 cross-linked with PEG – PMVE/MA and PMVE/MAH respectively. Following the core process outlined in Section 2.1, all materials were firstly prepared as required, poured on the front mould, and then positioned on the VT. The excess material was removed, the needles were either cured or dried, and then coupled with a substrate polymer and rear mould. Alternatively, the substrate material was pressed against the MNs after excess removal and the stack subsequently cured (see below).

Desirable properties for the substrate include biocompatibility and flexibility. Biocompatible polymers have been already demonstrated in the implementation of the core process [35]. Regardless of the polymer of choice, accredited testing should be undertaken to certify that the combination of materials used in the final device is biocompatible according to ISO 10993 standards for cytotoxicity, irritation, and skin sensitization. Flexibility can be implemented using a mouldable polymer, a flexible film or textile. The only constraint for the choice of the substrate material is that it must bond to the MN material. Three main materials were successfully used as flexible backing substrates: a low viscosity epoxy (Epotek 310 M from Epoxy Technology Europe Ltd, UK), a conductive fabric (NCS95R-CR from Marktek Inc, Chesterfield, USA) [10] and a thermoplastic polyurethane (TPU) sheet (ST604, Bemis Associates Inc, Shirley, USA) [55].

As mentioned during the description of the core moulding process, the epoxy was poured on the rear of the needles, the rear mould added and then the material was cured to form the hybrid wafer. Non-adhesive materials such as films or fabric must be applied to the mould before the microneedle material is cured or dried.

To demonstrate the capabilities of the platform to produce multi-materials arrays, a patch combining three different types of MNs was produce as shown in Fig. 7.

The array combines medical grade (Epotek 353ND, Fig. 7E), degradable (PVP-PVA loaded with methylene blue, Fig. 7D), and UV-curable (NOA 68 coloured with a red dye to highlight the different material, Fig. 7C) MNs. Two rows of seven needles were formed for each

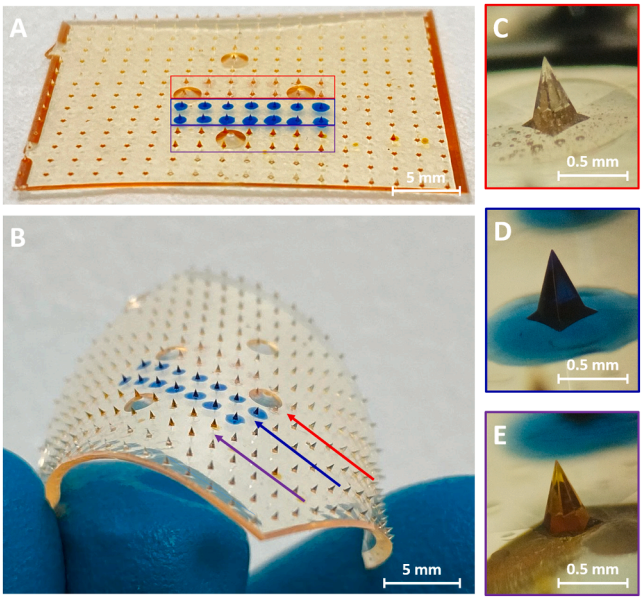

Fig. 7. MNs array (A and B) produced merging together different materials: a UV-curable polymer (NOA 68 - C), a methylene blue loaded PVP-PVA degradable mixture, and a medical grade epoxy (Epotek 353ND) were integrated on a flexible epoxy substrate (Epotek 310 M). The different MNs are highlighted using red, blue, and purple arrows, respectively.

material, also proving the spatial selectivity achievable with the platform. These needles were bonded to a flexible backing formed with Epotek 310 M.

2.5. Passivation and coating

In addition to all the aspects shown so far, some extra features, such as passivation of the array, functionalization of the needles, chlorination of the metal or sterilization of the patch may be needed for the intended application.

Passivation may be desirable for multiple purposes on MN-based devices: it is often used to geometrically define the areas of the electrodes [56], remove interferences coming from the array substrate or non-targeted body fluids [20], or selectively expose only part of the needle body [57]. MNs can be passivated using a variety of different techniques and materials, including spin-coating of different polymers such as OrmoComp [20] or polyimide [58], chemical vapour deposition (CVD) of parylene [57], or direct casting of varnish [35] or SU-8 [58]. We have further investigated, characterized and compared different passivation techniques in a previous work [39].

MNs can be coated for transdermal drug delivery [40,41], or be functionalised in a variety of different ways to detect specific biomarkers [9], antibodies [59], drugs [35], or characteristics such as skin pH [20]. Functionalization is the key to producing MN-based biosensors, which provides unique advantages due to their minimally invasive nature [42, 60]. An electrochemical sensor is usually comprised of one or more working electrodes (WEs), responsible for the detection of the desired biomarker, a counter electrode (CE) and a reference electrode (RE). The CE is used to apply the input potential to the WE [61] while the RE is needed to provide a constant potential to be used, as the name suggest, as a reference for the measurement [62]. Silver/silver-chloride (Ag/AgCl) is commonly used as a RE material, achieved by depositing Ag in various ways and then chlorinating it with Cl-based solutions [53, 63–65].

Because of the nature of their applications, sterility is an important consideration for MN devices. Several methods can be used as sterilization techniques, divided into those that require high temperatures, low temperatures or are based on the use of liquid chemicals. High temperature techniques can either use steam or dry heat while low temperature procedures use gasses, ozone, pulsed light or radiation [66]. Considering that our platform is based on polymer materials, usually vulnerable to high temperatures, the use of low temperature techniques is advised, and the effects of sterilisation procedures on the structural properties of the microneedles, as well as on the efficacy of the coating layers, should be thoroughly characterised.

3. Exemplars

The capabilities of the platform were demonstrated using three exemplars, each targeting one of the main medical application areas for MNs.

3.1. ELSAH biosensor

MNs have the potential to enable the next generation of wearable systems for minimally invasive continuous glucose monitoring [9]. The ELSAH project (funded from the European Union's Horizon 2020 research and innovation program under grant agreement No 825549) developed a MN-based, integrated wearable sensor system for simultaneous glucose and lactate detection in ISF. MN wafers based on Tyndall's MN template were produced using 7 g of Epotek 353ND; each wafer was divided into six 19 × 21 mm^2 rectangular biosensors. Custom metal masks were used to form two working electrodes (WEs), one counter electrode (CE) and one reference electrode (RE) on each sensor. Front-to-rear electrical connection was achieved by exploiting the conical through-wafer vias described earlier. Both WEs, the CE and the rear metallization were formed by depositing 20 nm of Ti and 100 nm of Pt whilst 30 nm of Ti, 60 nm of nickel (Ni) and 150 nm of silver (Ag) were used for the RE. The metal layers were all deposited using a Temescal EUFC4900 (Temescal, USA) e-beam evaporator. The RE was then chlorinated by exposing the Ag to a 15 % solution of sodium hypochlorite for 10 seconds. The solution was then washed away with ultrapure water and the sensor dried using a nitrogen gun. A fully metallized and chlorinated ELSAH biosensor wafer is shown in Fig. 8.

On each of the six sensors, a 5 × 1 MN RE is visible above two rectangular 5 × 2 MN WEs. A U-shaped CE is wrapped around them. Loctite EDAG 7019 (Henkel, Düsseldorf, Germany), a conductive Ag/

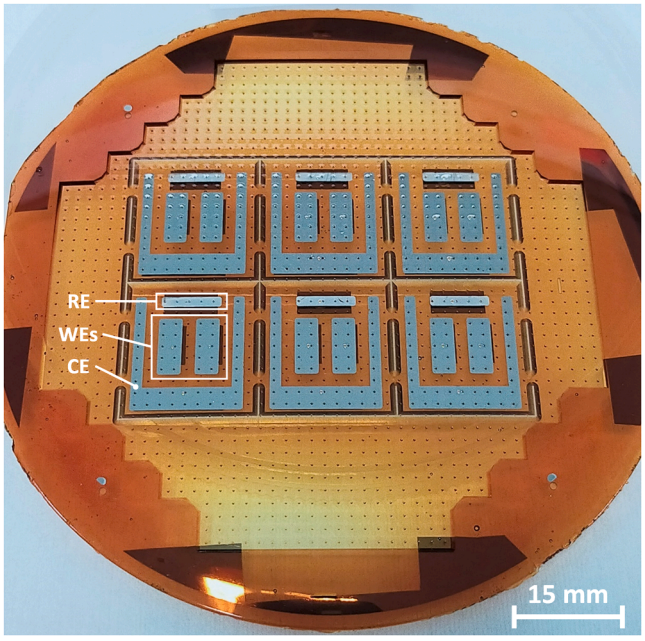

Fig. 8. An epoxy ELSAH wafer. All 6 biosensors have been metallized and the REs chlorinated.

AgCl ink, was used to fill the through-vias, ensuring a reliable front-to-rear electrical connection. The WEs were treated with a cysteamine hydrochloride solution (104 mg in a mixture of 7.6 ml physiological phosphate-buffered saline – PBS – solution and 2.4 ml glycerol) to improve the adhesion of the subsequent enzyme-based functionalization. For the passivation of the non-sensing areas, a medical grade tape (ARcare 7759, Adhesives Research, Limerick, Ireland), was cut to size and patterned with circular holes of diameter (760.4 ± 0.6 μm, n = 5) to match the MN pitch. A Speedy 360 laser cutter from Trotec (Marchtrenk, Austria) was used for cutting the tape. After manually applying the passivation, the sensors were ready for modification. Direct electron transfer (DET) enzymes Glucozyme and Lactazyme (developed and supplied by DirectSens GmbH Vienna, Austria) react with glucose and lactate respectively, and were added to two different poly(3,4-ethylenedioxythiophene) polystyrene sulfonate (PEDOT:PSS) inks formulated and deposited by AIT Austrian Institute of Technology GmbH (AIT, Vienna, Austria). A BioDOT AD1520 dispenser (BioDot Limited, Chichester, UK) was used to locally deposit the inks directly on the individual MNs. The deposited volume per WE was 150 nl for glucose detection (ink formulation: 38.3 μl water with 0.6 mg bovine serum albumin (BSA) and 4 mg Glucozyme, 89.4 μl PEDOT 1.1 % (w/w)) and 600 nl for lactate detection (ink formulation: 17 μl water, 13.2 μl PEDOT 1.1 % (w/w), 51.8 μl Lactazyme 7.9 mg ml^{-1} in water). Finally, a protective poly(ethylene glycol) dimethacrylate (PEG-DMA) based hydrogel layer [53] was dispensed on the needles using the BioDOT AD1520. This layer acted as a protective layer for the functionalization underneath [67]. 3 × 50 nl and 2 × 250 nl of hydrogel ink per needle were used for glucose and lactate modified WEs, respectively. After deposition, the ink was crosslinked using a UVP CL-1000 UV crosslinker (Analytic Jena US LLC, Upland, Canada), washed with PBS and dried under vacuum conditions. After the drying process, the hydrogel layer forms a stiff, thin (μm-range) layer on the microneedles, which swells when it comes in contact with ISF.

To be used on humans, the sensors must be sterilised, and the impact of sterilization was evaluated by preparing a batch of sensors, eight functionalised (both WEs) for glucose detection and eleven for lactate detection. Four sensors per type were then individually sealed inside an aluminium-coated bag together with a silica gel bag (1 g). The sensors were e-beam sterilized at 25 kGy by Mediscan GmbH (Seibersdorf, Austria). Before and after sterilization, the sensors were stored at 4 °C. The remaining control sensors were sealed in similar fashion and also stored at 4 °C. *In vitro* chronoamperometric measurements were performed on both sterilized and unsterilized biosensors. Solutions of glucose and lactate in PBS were used with concentrations varying between 0 and 30 mM, Fig. 9. A reduction in the maximum current of −49 % and −68 % after sterilisation can be observed for glucose and lactate biosensors respectively. Furthermore, a reduced current resolution compared to the unsterilized biosensors was detected. However, the final resolution of the glucose biosensors in the concentration range of 2.5–10 mM with 8 nA mM^{-1} and the final resolution of lactate biosensors in the range of 0–2.5 mM of 599 nA mM^{-1} will be sufficient to test ISF concentrations [68,69] in healthy volunteers during a planned *in vivo* study.

The difference between sterilized and non-sterilized sensors is caused by a reduction in enzyme activity. This has already been reported for microneedle-based biosensors with glucose oxidase sterilised by gamma irradiation with a dose of 25 kGy [70]. More recently, enzyme activity tests combined with circular dichroism showed that gamma irradiation induces a loss in enzyme activity in both glucose oxidase and cellobiose dehydrogenase (CDH) enzymes [71], used in this work. Also, it has been demonstrated that a very low irradiation flow rate (25 kGy applied at 260 Gy h^{-1} for 96 h instead of the standard 1670 Gy h^{-1} for 15 h) can help preserve the sensor performances [71]. Therefore, in preliminary tests, we compared the impact of 25 kGy e-beam and gamma irradiation at standard irradiation flow rates on the sensor performance/enzyme activity. E-beam irradiation had less impact, and it was consequentially chosen for this work.

Sensors were prepared for the volunteer study following the same protocol and glued with medical grade adhesive (Loctite 4011, Henkel, Düsseldorf, Germany) to a 3D printed disk, functionalised, and e-beam sterilised. The sensors were then inserted inside a 3D printed enclosure, interfaced with a printed circuit board for sensor readout and wireless communication, and tested for glucose and lactate detection on 30 healthy volunteers by the Medical University of Graz (MUG, Graz, Austria). Pictures of the system are shown in Fig. 10. The 3D printed disks and enclosures were produced by Sanmina (Fermoy, Ireland) using a Tough 1500 resin and a Form 3B printer (both from FormLabs GmbH, Berlin, Germany). A PCB, equipped with a potentiostat on chip, near field and ultra-high frequency communication (NFC and UHF respectively), was built by Infineon Technologies Austria (Villach, Austria) [72]. Full details of the study and associated data will be reported in a future publication.

3.2. Fabric-based ECG electrodes

Microneedle-based 'dry' electrodes have significant potential for use in biopotential recording applications because of their ability to create a low impedance interface with the skin and bypass some of the problems,

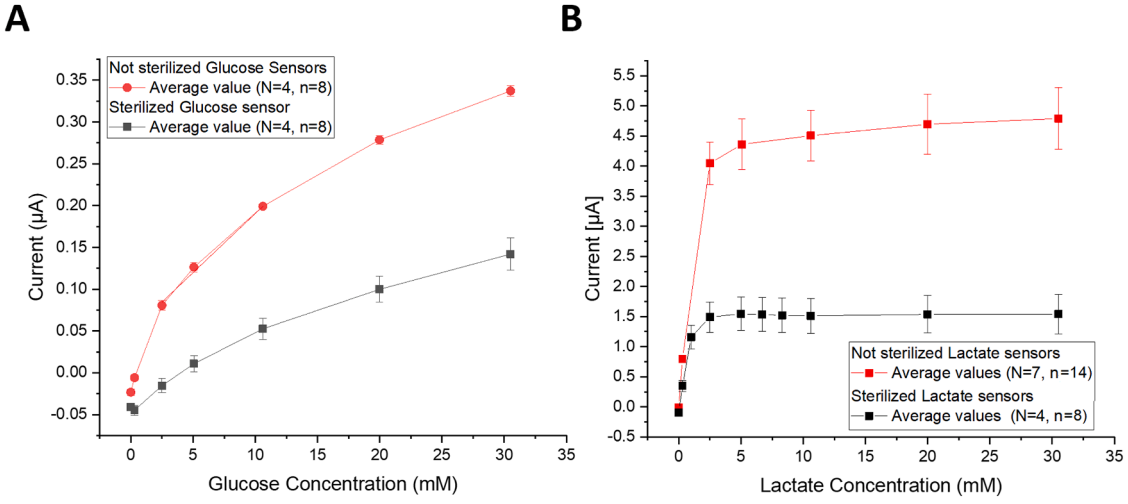

Fig. 9. Calibration curves of unsterilized and sterilized biosensors in the 0–30 mM glucose (A) and lactate (B) range in PBS solution. N represents the number of sensors used for testing and n the total number of modified WEs.

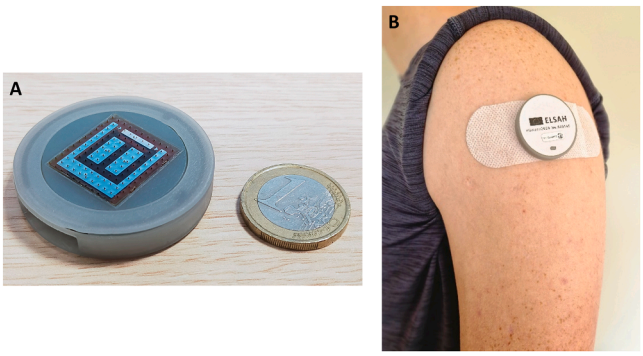

Fig. 10. ELSAH system used for in vitro testing (A) and final device affixed to the arm of a volunteer (B). There is no size difference between the testing device and the final device.

such as the need for skin abrasion, shaving and the use of a wet gel, that are associated with conventional gel-based electrodes [21]. Using the platform outlined earlier, we developed and characterised a flexible MN-based dry electrode for electrocardiogram (ECG) recording. Epotek 353ND was used to form the needles. As explained in Section 2.1, the front mould was placed on a VT and the excess material removed. A conductive fabric was patterned into 18 mm diameter circular electrodes and cut to shape to fit the needle mould. A Cricut Maker (from Cricut, South Jordan, USA) cutting machine was used for this operation. The fabric substrate was then pressed against the MNs mould, and the epoxy was cured at 80°C for 1 hour. Once peeled away from the mould, flexible electrodes with rigid MNs bonded to the conductive fabric were formed (Fig. 11A). 20 nm of Ti and 150 nm of Au were used to metallise the MN side of the newly formed arrays, while front-to-rear electrical connection was self-realised around the sides of the electrodes. For characterisation purposes, commercially available Red Dot 2239 electrodes (3 M, Ireland) were stripped of their gel pads and used to build the dry electrodes: the circular arrays were detached from the wafer and glued to the modified Red Dot with a medical grade conductive glue (Epotek Med-H20E from Epoxy Technology Inc, USA). The glue was cured according to manufacturer's instructions and the electrodes sterilised with a ProCleaner Plus (Bioforce Nanoscience, USA) ozone cleaner. To compare electrode performance with commercially available options, simultaneous recordings of ECG traces from commercial wet (Red Dot) and dry electrodes were acquired from healthy volunteers. This study was approved by the Clinical Research Ethics Committee of the Cork Teaching Hospitals (ref ECM 3 (ZZ) 10/11/20) and all participants provided written informed consent. A dual-channel ECG recording system was used to capture both signals in different static and walking conditions. An example of the two traces can be seen in Fig. 11B.

It is clear that the dry electrodes capture ECG signals with a similar level of fidelity to the commercial wet electrodes. Signal-to-noise ratios were in excess of 20 dB while sitting, and the P wave, QRS complex, and T wave of the ECG signal are clearly identifiable from both sets of electrodes. However, the dry electrodes do not require skin preparation or a wet gel, whilst providing a comparable level of signal quality and low electrode-skin impedance. Additional information and detailed analysis can be found in a previous work [10].

3.3. Transdermal delivery

Biodegradable or dissolvable microneedles (DMN) are the subject of intense research interest for applications in drug and vaccine delivery [8], and numerous DMNs moulded from the Tyndall template have been described in previous works [73,74]. These dissolvable materials and microneedles could also be used to protect labile medicants, thereby increasing their stability over a prolonged period. To test this hypothesis together with an evaluation of their delivery capabilities, different dissolvable MNs were produced following the process described in Section 2.1. In particular, TRA/SUC sugar needles, PVP/PVA polymer needles and PCL/PLGA polymer needles were fabricated.

The sugar needles, Fig. 12A and Fig. 12B, were used to test the stability of a macromolecule loaded inside the sugar glasses. To do that, a β-galactosidase enzyme was loaded inside a TRA/SUC dehydrated matrix and stored under vacuum desiccation conditions at 20 ± 2 °C and under refrigerated desiccation conditions at 4 ± 2 °C. The same enzyme was also loaded in dehydrated sodium phosphate buffer (PB) and used as a control. The residual enzyme activity was quantified at time points by a 2-nitrophenyl β-D-Galactopyranoside assay. The results, represented as means measured over 3 samples, are shown in Fig. 12C.

The testing demonstrated that, when loaded inside a sugar glass, more than 40 % of the enzyme activity was retained over a period of 3 months. On the other hand, the enzyme loaded inside the PB almost entirely denatured after dehydration. Additional information can be found in a previous work [75].

The PVP and PVA needles were produced using an Epotek 353ND circular MN array as a master (Fig. 13). The master itself was produced with the previously described moulding process, using a silicon wafer as a starting point. The mould was prefilled with a hyaluronic acid and niacinamide formulation before adding either the PVP, PVA or PVP/PVA, trapping the formulation inside the forming needles. These actives are used in the management of dermatological conditions such as acne or atopic dermatitis [76,77]. These needles were tested on full thickness porcine skin and were able to successfully deliver over 150 μg cm^{-2} of drug over a 24-hour period [78].

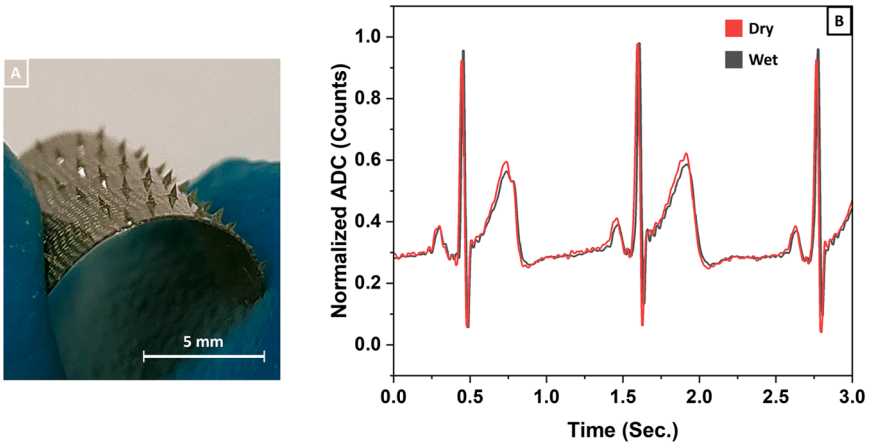

Fig. 11. Conductive cloth-epoxy hybrid electrode (A) together with simultaneous ECG recordings from wet and dry electrodes (B).

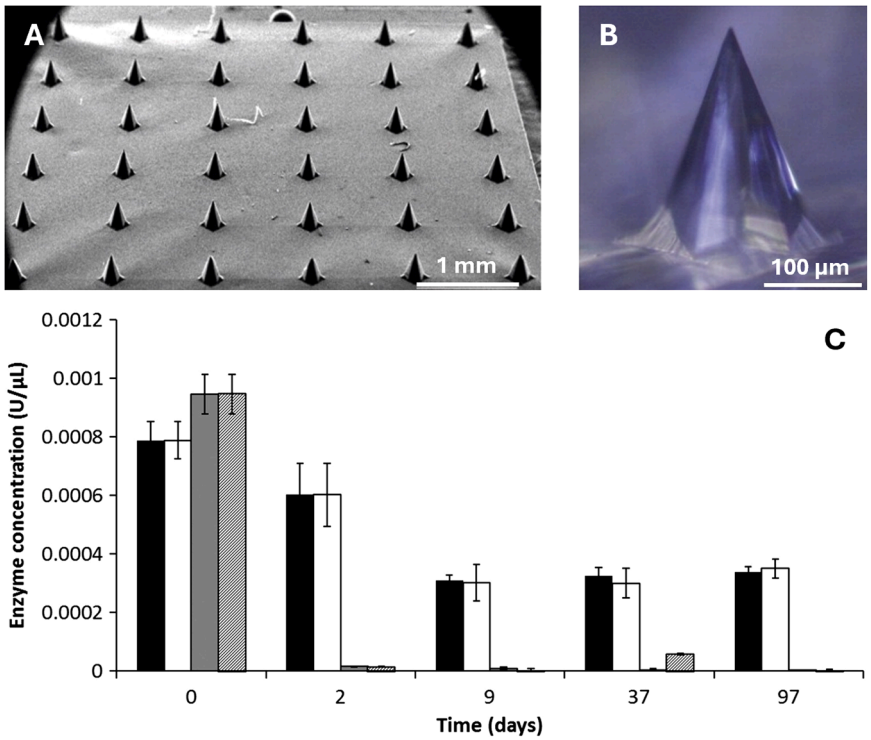

Fig. 12. Scanning electron micrograph of an entire sugar glass microneedle array (a) together with a light photomicrograph of an individual sugar glass microneedle (B). Assessment of enhanced biomolecule stability within sugar glasses as a function of different storage conditions (C). The β-galactosidase enzyme was incorporated either within solid sugar glass (black and white bars) or in a lyophilised phosphate buffer (dark grey and light grey striped bars). Samples were stored under vacuum desiccation at 20 ± 2 °C (white and stripped bars) or desiccation at 4 ± 2 °C (black and grey bars) for a period of 3 months. All images in Fig. 12 (A-C) are reproduced with permission [75]. Copyright 2011, Elsevier B.V.

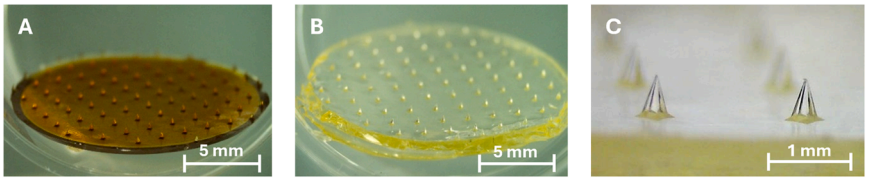

Fig. 13. Epoxy master (A) together with resulting PVP array (B), and a close up picture of two similarly prepared PVA microneedles (C).

Both the sugar and the PVP/PVA needles were fast dissolving needles. To demonstrate the ability of the platform to produce slow dissolving MNs, PCL, PLGA and PCL/PLGA needles were also produced and tested on skin samples to prove their ability to penetrate the skin. PCL/PLGA MNs are reported in Fig. 14 together with an image showing penetration marks on a skin sample.

Human factors studies also indicate that microneedle-based treatments such as these would be well received by patients, who value its convenience, minimally invasive nature and the potential for self-administration [79,80].

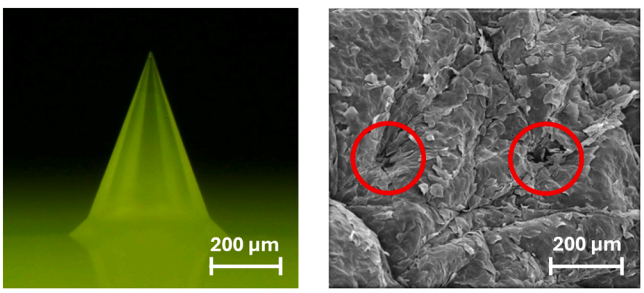

Fig. 14. Microneedles prepared from a blend of PCL and PLGA (A) together with a SEM picture showing penetration marks (red circles) produced by MNs application (B).

4. Conclusions

A multifunctional platform for the rapid prototyping and production of polymer microneedle arrays was established and characterized. The shape, dimension and number of arrays can be varied simply by designing the front and rear master templates accordingly. In this double-sided process, the front template is used to define the geometry, pitch and height of the microneedles themselves, while the rear template shapes the arrays as well as additional features, such as electrical through-wafer vias and alignment marks. The polymer is chosen according to the properties required for the final application. One or more materials may be used to form the MNs and the substrate, or even integrated to combine different properties on single arrays. The moulded MNs can be customised for various sensing applications by using different techniques to deposit metal, passivation and electrochemical layers as required. Sputtering and e-beam evaporation have been characterized and employed to produce patterned electrodes and sensors, and shadow masking techniques have been developed to accurately deposit electrically active regions while preventing the undesirable

'spreading' of metal beneath the masks. Three different exemplars were described, including an electrochemical biosensor for transdermal diagnostics, a flexible ECG sensor, and a biodegradable drug delivery array. These examples illustrate how easily the process may be adapted to a wide range of use cases, making it highly valuable for prototyping and research purposes.

Funding sources

This publication has emanated from research conducted with the financial support of the European Union's Horizon 2020 Research and Innovation Programme under grant #825549 (ELSAH project); the Government of Ireland through the Disruptive Technologies Innovation Fund (DT2018 0291-A, HOLISTICS); Research Ireland through the Insight Centre for Data Analytics (SFI/12/RC/2289-P2); Enterprise Ireland under the Commercialisation Fund (CF/2012/2339); the Higher Education Authority under the Programme for Research in Third-Level Institutions; and the European Regional Development Fund. Martin's PhD was funded by 3 M. Ng's PhD was funded by the School of Pharmacy and Pharmaceutical Sciences, Cardiff University and the Overseas Research Students Awards Scheme (ORSAS). Massufero Vergilio's PhD internship was funded by Santander Open Academy.

For the purpose of Open Access, the author has applied a CC BY public copyright licence to any Author Accepted Manuscript version arising from this submission. Open access funding is provided by IReL.

CRediT authorship contribution statement

Birchall James: Funding acquisition, Investigation, Writing – review & editing. **Donovan Paul:** Writing – review & editing, Methodology, Visualization. **Bocchino Andrea:** Conceptualization, Data curation, Formal analysis, Investigation, Methodology, Validation, Writing – original draft, Writing – review & editing, Visualization. **Mutinati Giorgio C.:** Funding acquisition, Investigation, Project administration, Resources, Writing – review & editing. **Coulman Sion:** Data curation, Investigation, Methodology, Writing – review & editing. **Martin Christopher:** Data curation, Investigation, Methodology, Writing – review & editing. **Ng Keng Wooi:** Data curation, Investigation, Methodology, Writing – review & editing. **Galvin Paul:** Project administration, Resources, Supervision, Writing – review & editing. **Marquez-Grana Carlota:** Data curation, Investigation, Methodology, Validation, Writing – review & editing. **O'Mahony Conor:** Conceptualization, Funding acquisition, Investigation, Methodology, Project administration, Resources, Supervision, Writing – review & editing. **Singh Om Prakash:** Data curation, Investigation, Methodology, Validation, Writing – review & editing, Visualization. **Melnik Eva:** Data curation, Investigation, Methodology, Writing – review & editing, Visualization. **Kurzhals Steffen:** Data curation, Investigation, Methodology, Visualization, Writing – review & editing. **Massufero Vergilio Mariane:** Data curation, Investigation, Methodology, Writing – review & editing.

Declaration of Competing Interest

The authors declare no conflict of interest.

Acknowledgements

The authors would like to thank UpNano GmbH, Boston Micro Fabrication (BMF) and Johannes Kepler University Linz for the provision of microneedle samples.

Appendix A. Supporting information

Supplementary data associated with this article can be found in the online version at doi:10.1016/j.sna.2025.116491.

Data availability

Data will be made available on request.

References

[1] F.K. Aldawood, A. Andar, S. Desai, A comprehensive review of microneedles: types, materials, processes, characterizations and applications, Polymers 13 (2021) 2815, https://doi.org/10.3390/polym13162815.
[2] C. Czekalla, K.H. Schönborn, J. Lademann, M.C. Meinke, Noninvasive determination of epidermal and stratum corneum thickness in vivo using two-photon microscopy and optical coherence tomography: impact of body area, age, and gender, Ski. Pharmacol. Physiol. 32 (2019) 142–150, https://doi.org/10.1159/000497475.
[3] Histology, Stratum Corneum, StatPearls. ⟨http://www.ncbi.nlm.nih.gov/books/NBK513299/⟩, 2023 (accessed 8 January 2024).
[4] J. Wang, z Lu, R. Cai, H. Zheng, J. Yu, Y. Zhang, Z. Gu, Microneedle-based transdermal detection and sensing devices, Lab. Chip 23 (2023) 869–887, https://doi.org/10.1039/D2LC00790H.
[5] M. Zheng, T. Sheng, J. Yu, Z. Gu, C. Xu, Microneedle biomedical devices, Nat. Rev. Bioeng. 2 (2023) 324–342, https://doi.org/10.1038/s44222-023-00141-6.
[6] R. Parhi, D. S. N, Review of microneedle based transdermal drug delivery systems, Int. J. Pharm. Sci. Nanotechnol. 12 (2019) 4511–4523, https://doi.org/10.37285/ijpsn.2019.12.3.1.
[7] T. Waghule, G. Singhvi, S.K. Dubey, M.M. Pandey, G. Gupta, M. Singh, K. Dua, Microneedles: a smart approach and increasing potential for transdermal drug delivery system, Biomed. Pharm. 109 (2019) 1249–1258, https://doi.org/10.1016/j.biopha.2018.10.078.
[8] I. Menon, P. Bagwe, K.B. Gomes, L. Bajaj, R. Gala, M.N. Uddin, M.J. D'Souza, S. M. Zughaier, Microneedles: a new generation vaccine delivery system, Micromachines 12 (2021) 435, https://doi.org/10.3390/mi12040435.
[9] J. Madden, C. O'Mahony, M. Thompson, A. O'Riordan, P. Galvin, Biosensing in dermal interstitial fluid using microneedle based electrochemical devices, Sens. Bio-Sens. Res. 29 (2020) 100348, https://doi.org/10.1016/j.sbsr.2020.100348.
[10] O.P. Singh, A. Bocchino, T. Guillerm, Y. Hu, F. Stam, C. O'Mahony, Flexible, conductive fabric-backed, microneedle electrodes for electrophysiological monitoring, Adv. Mater. Technol. 9 (2023) 2301606, https://doi.org/10.1002/admt.202301606.
[11] M. O'Sullivan, A. Temko, A. Bocchino, C. O'Mahony, G. Boylan, E. Popovici, Analysis of a low-cost EEG monitoring system and dry electrodes toward clinical use in the neonatal ICU (Article), Sensors 19 (11) (2019), https://doi.org/10.3390/s19112637.
[12] A.T. Satti, J. Kim, E. Yi, H.-Y. Cho, S. Cho, Microneedle array electrode-based wearable EMG system for detection of driver drowsiness through steering wheel grip, Sensors 21 (2021) 5091, https://doi.org/10.3390/s21155091.
[13] H. Zhang, H. Zhao, X. Zhao, C. Xu, D. Franklin, A. Vázquez-Guardado, W. Bai, J. Zhao, K. Li, G. Monti, W. Lu, A. Kobeissi, L. Tian, X. Ning, X. Yu, S. Mehta, D. Chanda, Y. Huang, S. Xu, B.E.P. White, J.A. Rogers, Biocompatible light guide-assisted wearable devices for enhanced UV light delivery in deep skin, Adv. Funct. Mater. 31 (2021), https://doi.org/10.1002/adfm.202100576.
[14] C. O'Mahony, R. Houlihan, K. Grygoryev, Z. Ning, J. Williams, T. Moore, Design, modelling and preliminary characterisation of microneedle-based electrodes for tissue electroporation in vivo, J. Phys. Conf. Ser. 757 (2016) 012040, https://doi.org/10.1088/1742-6596/757/1/012040.
[15] A. Tucak, M. Sirbubalo, L. Hindija, O. Rahić, J. Hadžiadvić, K. Muhamedagić, A. Čekić, E. Vranić, Microneedles: characteristics, materials, production methods and commercial development, Micromachines 11 (2020) 961, https://doi.org/10.3390/mi11110961.
[16] N. Gan, M. Wei, Q. Zhou, K. Dong, B. Gao, Silk fibroin-based trielectric nanogenerators for energy harvesting and biomedical applications, ACS Appl. Nano Mater. (8) (2024) 8407–8423, https://doi.org/10.1021/acsanm.4c00335.
[17] C. O'Mahony, A. Bocchino, M.J. Haslinger, D. Fechtig, K. Schossleitner, P. Galvin, S. Brandstätter, Characterisation of microneedle-based ECG electrodes fabricated using an industrial injection-moulding process. in: Proc. - IEEE Int. Conf. Micro Elec. Mech. Syst, IEEE, 2019, pp. 557–560, https://doi.org/10.1109/MEMSYS.2019.8870721.
[18] K. Schossleitner, C. O'Mahony, S. Brandstätter, M.J. Haslinger, S. Demuth, D. Fechtig, P. Petzelbauer, Differences in biocompatibility of microneedles from cyclic olefin polymers with human endothelial and epithelial skin cells, J. Biomed. Mater. Res. A 107 (2019) 505–512. ⟨https://doi.org/10.1002/jbm.a.36565⟩.
[19] M. Wang, L. Hu, C. Xu, Recent advances in the design of polymeric microneedles for transdermal drug delivery and biosensing, Lab. Chip 17 (2017) 1373–1387. ⟨https://doi.org/10.1039/C7LC00016B⟩.
[20] M. Dervisevic, E. Dervisevic, L. Esser, C.D. Easton, V.J. Cadarso, N.H. Voelcker, Wearable microneedle array-based sensor for transdermal monitoring of pH levels in interstitial fluid, Biosens. Bioelectron. 222 (2023) 114955. ⟨https://doi.org/10.1016/j.bios.2022.114955⟩.
[21] Y. Hou, Z. Li, Z. Wang, H. Yu, Miura-ori structured flexible microneedle array electrode for biosignal recording, Article 1, Microsyst. Nanoeng. 7 (2021), https://doi.org/10.1038/s41378-021-00259-w.
[22] M.J. Uddin, N. Scoutaris, S.N. Economidou, C. Giraud, B.Z. Chowdhry, R. F. Donnelly, D. Douroumis, 3D printed microneedles for anticancer therapy of skin tumours, Mater. Sci. Eng. C. 107 (2020) 110248. ⟨https://doi.org/10.1016/j.msec.2019.110248⟩.

[23] M.A. Luzuriaga, D.R. Berry, J.C. Reagan, R.A. Smaldone, J.J. Gassensmith, Biodegradable 3D printed polymer microneedles for transdermal drug delivery, Lab. Chip 18 (2018) 1223–1230. ⟨https://doi.org/10.1039/C8LC00098K⟩.

[24] J. Li, Z. Shen, H. Wang, D. Huang, Y. Chen, Q. Mou, Low-cost, low-impedance polyimide based micro-needle array (PI-MNA): a minimally invasive flexible dry electrode for surface bio-potential monitoring. in: Proc. - IEEE Int. Conf. Micro Electro Mech. Syst, IEEE, 2019, pp. 28–31, https://doi.org/10.1109/MEMSYS.2019.8870653.

[25] Z. Chen, L. Ren, J. Li, L. Yao, Y. Chen, L. Jiang, Rapid fabrication of microneedles using magnetorheological drawing lithography, Acta Biomater. 65 (2018) 283–291, https://doi.org/10.1016/j.actbio.2017.10.030.

[26] P. Bollella, S. Sharma, A.E.G. Cass, R. Antiochia, Microneedle-based biosensor for minimally-invasive lactate detection, Biosens. Bioelectron. 123 (2019) 152–159, https://doi.org/10.1016/j.bios.2018.08.010.

[27] L. Ren, S. Xu, J. Gao, Z. Lin, Z. Chen, B. Liu, L. Liang, L. Jiang, Fabrication of flexible microneedle array electrodes for wearable bio-signal recording (Article), Sensors 18 (4) (2018), https://doi.org/10.3390/s18041191.

[28] M. Zheng, Z. Wang, H. Chang, L. Wang, S.W.T. Chew, D.C.S. Lio, M. Cui, L. Liu, B. C.K. Tee, C. Xu, Osmosis-powered hydrogel microneedles for microliters of skin interstitial fluid extraction within minutes, Adv. Healthc. Mater. 9 (2020) 1901683, https://doi.org/10.1002/adhm.201901683.

[29] R.F. Donnelly, M.T.C. McCrudden, A.Z. Alkilani, E. Larrañeta, E. McAlister, A. J. Courtenay, M.-C. Kearney, T.R.R. Singh, H.O. McCarthy, V.L. Kett, E. Caffarel-Salvador, S. Al-Zahrani, A.D. Woolfson, Hydrogel-forming microneedles prepared from "super swelling" polymers combined with lyophilised wafers for transdermal drug delivery, PLoS ONE 9 (2014) e111547, https://doi.org/10.1371/journal.pone.0111547.

[30] S. Sharma, Z. Huang, M. Rogers, M. Boutelle, A.E.G. Cass, Evaluation of a minimally invasive glucose biosensor for continuous tissue monitoring, Anal. Bioanal. Chem. 408 (2016) 8427–8435, https://doi.org/10.1007/s00216-016-9961-6.

[31] S.C. Park, M.J. Kim, S.-K. Baek, J.-H. Park, S.-O. Choi, Spray-formed layered polymer microneedles for controlled biphasic drug delivery, Article 2, Polymers 11 (2019), https://doi.org/10.3390/polym11020369.

[32] W. Li, R.N. Terry, J. Tang, M.R. Feng, S.P. Schwendeman, M.R. Prausnitz, Rapidly separable microneedle patch for the sustained release of a contraceptive, Article 3, Nat. Biomed. Eng. 3 (2019), https://doi.org/10.1038/s41551-018-0337-4.

[33] Y. Park, J. Park, G.S. Chu, K.S. Kim, J.H. Sung, B. Kim, Transdermal delivery of cosmetic ingredients using dissolving polymer microneedle arrays, Biotechnol. Bioprocess Eng. 20 (2015) 543–549, https://doi.org/10.1007/s12257-014-0775-0.

[34] F. Pérennès, B. Marmiroli, M. Matteucci, M. Tormen, L. Vaccari, E.D. Fabrizio, Sharp beveled tip hollow microneedle arrays fabricated by LIGA and 3D soft lithography with polyvinyl alcohol, J. Micromech. Microeng. 16 (2006) 473, https://doi.org/10.1088/0960-1317/16/3/001.

[35] S.A.N. Gowers, D.M.E. Freeman, T.M. Rawson, M.L. Rogers, R.C. Wilson, A. H. Holmes, A.E. Cass, D. O'Hare, Development of a minimally invasive microneedle-based sensor for continuous monitoring of β-lactam antibiotic concentrations in vivo, ACS Sens 4 (2019) 1072–1080, https://doi.org/10.1021/acssensors.9b00288.

[36] Y. Nishinaka, R. Jun, G.S. Prihandana, N. Miki, Fabrication of polymeric dry microneedle electrodes coated with nanoporous parylene. in: Proc. - IEEE Trans. Eurosens. XXVII: Int. Conf. Solid-State Sens. Act. Microsyst, IEEE, 2013, pp. 1326–1327, https://doi.org/10.1109/Transducers.2013.6627021.

[37] M. Wei, Q. Zhou, X. Ma, B. Gao, Review of biomimetic ordered microstructures in advancing synergistic integration of adhesion and microfluidics, RSC Adv. 14 (2024) 11643–11658, https://doi.org/10.1039/D3RA07698A.

[38] C. O'Mahony, K. Grygoryev, A. Ciarlone, G. Giannoni, A. Kenthao, P. Galvin, Design, fabrication and skin-electrode contact analysis of polymer microneedle-based ECG electrodes, J. Micromech. Microeng. 26 (2016) 084005, https://doi.org/10.1088/0960-1317/26/8/084005.

[39] A. Bocchino, S.R. Teixeira, S. Iadanza, E. Melnik, S. Kurzhals, G.C. Mutinati, Development and characterization of passivation methods for microneedle-based biosensors. in Proc. - IEEE Int. Conf. IEEE Eng. Med. Bio. Soc., IEEE, 2022, pp. 1275–1278, https://doi.org/10.1109/EMBC48229.2022.9871005.

[40] K.A.S. AL-Japairai, S. Mahmood, S.H. Almurisi, J.R. Venugopal, A.R. Hilles, M. Azmana, S. Raman, Current trends in polymer microneedle for transdermal drug delivery, Int. J. Pharm. 587 (2020) 119673, https://doi.org/10.1016/j.ijpharm.2020.119673.

[41] R.S.J. Ingrole, H.S. Gill, Microneedle coating methods: a review with a perspective, J. Pharmacol. Exp. Ther. 370 (2019) 555–569, https://doi.org/10.1124/jpet.119.258707.

[42] P. Dardano, I. Rea, L. De Stefano, Microneedles-based electrochemical sensors: new tools for advanced biosensing, Curr. Opin. Electrochem 17 (2019) 121–127, https://doi.org/10.1016/j.coelec.2019.05.012.

[43] O. Ojuroye, R. Torah, S. Beeby, Modified PDMS packaging of sensory e-textile circuit microsystems for improved robustness with washing, Microsyst. Technol. 28 (2022) 1467–1484, https://doi.org/10.1007/s00542-019-04455-7.

[44] R.V. Dixon, E. Skaria, W.M. Lau, P. Manning, M.A. Birch-Machin, S.M. Moghimi, K. W. Ng, Microneedle-based devices for point-of-care infectious disease diagnostics, Acta Pharm. Sin. B 11 (2021) 2344–2361, https://doi.org/10.1016/j.apsb.2021.02.010.

[45] A.S. Cordeiro, I.A. Tekko, M.H. Jomaa, L. Vora, E. McAlister, F. Volpe-Zanutto, M. Nethery, P.T. Baine, N. Mitchell, D.W. McNeill, R.F. Donnelly, Two-photon polymerisation 3D printing of microneedle array templates with versatile designs: application in the development of polymeric drug delivery systems, Pharm. Res. 37 (2020) 174, https://doi.org/10.1007/s11095-020-02887-9.

[46] C. Plamadeala, S.R. Gosain, F. Hischen, B. Buchroithner, S. Puthukodan, J. Jacak, A. Bocchino, D. Whelan, C. O'Mahony, W. Baumgartner, J. Heitz, Bio-inspired microneedle design for efficient drug/vaccine coating, Biomed. Micro 22 (2019) 8, https://doi.org/10.1007/s10544-019-0456-z.

[47] C. O'Mahony, Structural characterization and in-vivo reliability evaluation of silicon microneedles, Biomed. Micro 16 (2014) 333–343, https://doi.org/10.1007/s10544-014-9836-6.

[48] D. Kulkarni, F. Damiri, S. Rojekar, M. Zehravi, S. Ramproshad, D. Dhoke, S. Musale, A.A. Mulani, P. Modak, R. Paradhi, J. Vitore, H. Rahman, M. Berrada, P. S. Giram, S. Cavalu, Recent advancements in microneedle technology for multifaceted biomedical applications (Article), Pharmaceutics 14 (5) (2022), https://doi.org/10.3390/pharmaceutics14051097.

[49] R.J. Martín-Palma, A. Lakhtakia, Chapter 15 - Vapor-Deposition Techniques, in: A. Lakhtakia, R.J. Martín-Palma (Eds.), in Engineered Biomimicry, Elsevier, Boston, 2013, pp. 383–398, https://doi.org/10.1016/B978-0-12-415995-2.00015-5.

[50] A. Tamayo-Dominguez, P. Sanchez-Olivares, A. Camacho-Hernandez, J.-M. Fernandez-Gonzalez, Guidelines for accurate in-house electroplating and 3-D-printing processes applied to mm-wave devices, IEEE Microw. Wirel. Compon. Lett. 32 (2022) 1267–1270, https://doi.org/10.1109/LMWC.2022.3182868.

[51] A.S.H. Makhlouf, R. Rodriguez, Chapter 15 - Bioinspired smart coatings and engineering materials for industrial and biomedical applications, in: A.S. H. Makhlouf, N.Y. Abu-Thabit (Eds.), Advances in Smart Coatings and Thin Films for Future Industrial and Biomedical Engineering Applications, Elsevier, Amsterdam, 2020, pp. 407–427, https://doi.org/10.1016/B978-0-12-849870-5.00018-5.

[52] R.K. Kummamuru, L. Hu, L. Cook, M.Y. Efremov, E.A. Olson, L.H. Allen, A close proximity self-aligned shadow mask for sputter deposition onto a membrane or cavity, J. Micromech. Microeng. 18 (2008) 095027, https://doi.org/10.1088/0960-1317/18/9/095027.

[53] S. Kurzhals, E. Melnik, P. Plata, E. Cihan, P. Herzog, A. Felice, A. Bocchino, C. O'Mahony, G.C. Mutinati, R. Hainberger, Detection of lactate via amperometric sensors modified with direct electron transfer enzyme containing PEDOT:PSS and hydrogel inks, IEEE Sens. Lett. 7 (2023) 1–4, https://doi.org/10.1109/LSENS.2023.3307066.

[54] C. Barrett, K. Dawson, C. O'Mahony, A. O'Riordan, Development of low cost rapid fabrication of sharp polymer microneedles for in vivo glucose biosensing applications, ECS J. Solid State Sci. Technol. 4 (2015) S3053, https://doi.org/10.1149/2.0141510jss.

[55] O.P. Singh, A. Bocchino, T. Guillerm, C. O'Mahony, Design, fabrication and performance assessment of flexible, microneedle–based electrodes for ECG signal monitoring. in: Proc. - IEEE Int. Conf. IEEE Eng. Med. Bio. Soc., IEEE, 2022, pp. 846–849, https://doi.org/10.1109/EMBC48229.2022.9871073.

[56] C. Hegarty, A. McConville, R.J. McGlynn, D. Mariotti, J. Davis, Design of composite microneedle sensor systems for the measurement of transdermal pH, Mater. Chem. Phys. 227 (2019) 340–346, https://doi.org/10.1016/j.matchemphys.2019.01.052.

[57] D. Terutsuki, S. Yamaguchi, Y. Abe, H. Abe, M. Nishizawa, Porous microneedle-based potentiometric sensor for intradermal electrolyte monitoring, Electrochemistry 91 (2023) 047007, https://doi.org/10.5796/electrochemistry.23-00027.

[58] S. Metz, M.O. Heuschkel, B. Valencia Avila, R. Holzer, D. Bertrand, Ph Renaud, Microelectrodes with three-dimensional structures for improved neural interfacing. in: Proc. - IEEE Int. Conf. IEEE Eng. Med. Bio. Soc, IEEE, 2001, pp. 765–768, https://doi.org/10.1109/IEMBS.2001.1019053.

[59] Microneedle-based device for biological analysis, Frontiers. ⟨https://www.frontiersin.org/articles/10.3389/fbioe.2022.851134⟩, 2022 (accessed 16 January 2023).

[60] H. Abdullah, T. Phairatana, I. Jeerapan, Tackling the challenges of developing microneedle-based electrochemical sensors, Mikrochim. Acta 189 (2022) 440, https://doi.org/10.1007/s00604-022-05510-3.

[61] K.C. Honeychurch, 13 - Printed thick-film biosensors, in: M. Prudenziati, J. Hormadaly (Eds.), Printed Films, Woodhead Publishing Series in Electronic and Optical Materials, Woodhead Publishing, Sawston, 2012, pp. 366–409, https://doi.org/10.1533/9780857096210.2.366.

[62] P. Kurzweil, Electrochemical terminology | Electrochemical Cell Nomenclature, in: J. Garche (Ed.), Encyclopedia of Electrochemical Power Source (Second Edition, Elsevier, Amsterdam, 2025, pp. 449–464, https://doi.org/10.1016/B978-0-323-96022-9.00035-9.

[63] X. Huang, S. Zheng, B. Liang, M. He, F. Wu, J. Yang, H.-J. Chen, X. Xie, 3D-assembled microneedle ion sensor-based wearable system for the transdermal monitoring of physiological ion fluctuations, Article 25, Micro Nanoeng. 9 (2023), https://doi.org/10.1038/s41378-023-00497-0.

[64] J. Ju, L. Li, S. Regmi, X. Zhang, S. Tang, Microneedle-based glucose sensor platform: from vitro to wearable point-of-care testing systems, Biosensors 12 (2022) 606, https://doi.org/10.3390/bios12080606.

[65] D.S. Macedo, M. Vepsäläinen, D. Acharya, C.D. Wood, D. Wen, L. Thomson, S. Peacock, T. Rodopoulos, C.F. Hogan, An unusually stable solid state Ag|AgCl reference electrode for long term continuous measurements based on a crosslinked poly(vinyl acetate)/KCl composite, Electrochim. Acta 368 (2021) 137636, https://doi.org/10.1016/j.electacta.2020.137636.

[66] S. Mohapatra, Chapter 59 - Sterilization and Disinfection, in: H. Prabhakar (Ed.), Essentials of Neuroanesthesia, Academic Press, Cambridge, 2017, pp. 929–944, https://doi.org/10.1016/B978-0-12-805299-0.00059-2.

[67] E. Cihan, E. Melnik, S. Kurzhals, P. Plata, G.C. Mutinati, R. Hainberger, A.K. G. Felice, C. Schulz, P. Lieberzeit, Novel approach for the immobilization of cellobiose dehydrogenase in PEDOT:PSS conductive layer on planar gold

electrodes, Article 3, Chemosensors 12 (2024), https://doi.org/10.3390/chemosensors12030036.
[68] D.K. Ming, S. Jangam, S.A.N. Gowers, R. Wilson, D.M.E. Freeman, M.G. Boutelle, A. E.G. Cass, D. O'Hare, A.H. Holmes, Real-time continuous measurement of lactate through a minimally invasive microneedle patch: a phase I clinical study, BMJ Innov. 8 (2022) 87–94, https://doi.org/10.1136/bmjinnov-2021-000864.
[69] D.M.E. Freeman, D.K. Ming, R. Wilson, P.L. Herzog, C. Schulz, A.K.G. Felice, Y.-C. Chen, D. O'Hare, A.H. Holmes, A.E.G. Cass, Continuous measurement of lactate concentration in human subjects through direct electron transfer from enzymes to microneedle electrodes, ACS Sens 8 (2023) 1639–1647, https://doi.org/10.1021/acssensors.2c02780.
[70] S. Sharma, Z. Huang, M. Rogers, M. Boutelle, A.E.G. Cass, Evaluation of a minimally invasive glucose biosensor for continuous tissue monitoring, Anal. Bioanal. Chem. 408 (2016) 8427–8435, https://doi.org/10.1007/s00216-016-9961-6.
[71] R. Bennet, A. Rathore, S. Gounel, A. Lielpetere, T.M.B. Reichhart, K. Jayakumar, R. Ludwig, A.K.G. Felice, D. Leech, W. Schuhmann, A. Mount, N. Mano, C. Boiziau, Effects of sterilization on cellobiose dehydrogenase and glucose oxidase based glucose biosensors, Adv. Sens. Res. 3 (2024) 2400056, https://doi.org/10.1002/adsr.202400056.
[72] M. Haberler, I. Siegl, C. Zajc, C. Kollegger, C. Steffan, T. Maier, L. Petruzzi, G. Mutinati, R. Hainberger, G. Holweg, M. Auer, A self-contained, single-chip amperometric measurement platform for biomedical applications. in: Proc. - IEEE Int. Conf. Telecom, IEEE, 2021, pp. 105–109, https://doi.org/10.23919/ConTEL52528.2021.9495989.
[73] Y. Tian, J. Lee, K. van der Maaden, Y. Bhide, J.J. de Vries-Idema, R. Akkerman, C. O'Mahony, W. Jiskoot, H.W. Frijlink, A.L.W. Huckriede, W.L.J. Hinrichs, J. A. Bouwstra, M. Beukema, Intradermal administration of influenza vaccine with trehalose and pullulan-based dissolving microneedle arrays, J. Pharm. Sci. 111 (2022) 1070–1080, https://doi.org/10.1016/j.xphs.2022.01.033.
[74] J. Lee, M. Beukema, O.A. Zaplatynska, C. O'Mahony, W.L.J. Hinrichs, A.L. W. Huckriede, J.A. Bouwstra, K. van der Maaden, Efficient fabrication of thermostable dissolving microneedle arrays for intradermal delivery of influenza whole inactivated virus vaccine, Biomater. Sci. 11 (2023) 6790–6800, https://doi.org/10.1039/d3bm00377a.
[75] C.J. Martin, C.J. Allender, K.R. Brain, A. Morrissey, J.C. Birchall, Low temperature fabrication of biodegradable sugar glass microneedles for transdermal drug delivery applications, J. Control. Release 158 (2012) 93–101, https://doi.org/10.1016/j.jconrel.2011.10.024.
[76] J. Mehrabi, W. Shehadeh, E.S. Gallo, O. Artzi, T. Horovitz, Comparison of 2 hyaluronic acid-based fillers for the treatment of acne scars: structural lifting versus biostimulatory effect, Dermatol. Surg. 49 (2023) 581–586, https://doi.org/10.1097/DSS.0000000000003789.
[77] J.-R. Zhu, J. Wang, S.-S. Wang, A single-center, randomized, controlled study on the efficacy of niacinamide-containing body emollients combined with cleansing gel in the treatment of mild atopic dermatitis, Ski. Res. Technol. 29 (2023) e13475, https://doi.org/10.1111/srt.13475.
[78] M. Massufero-Vergilio, G.R. Leonardi, J.C. Birchall, Dissolvable microneedle array for enhanced niacinamide application for skin disorders, Submitted to: J. Drug. Deliv. Sci. Technol., January 2025.
[79] J.C. Birchall, R. Clemo, A. Anstey, D.N. John, Microneedles in clinical practice - an exploratory study into the opinions of healthcare professionals and the public, Pharm. Res. 28 (2011) 95–106, https://doi.org/10.1007/s11095-010-0101-2.
[80] B. Gualeni, L. Hughes, I. Stauber, L. Ackers, A. Gorman, D. Gashuga, N. Dzabala, F. Chimimba, I. Chikowe, S.A. Coulman, J.C. Birchall, Human-centred design of a new microneedle-based hormonal contraceptive delivery system, Gates Open Res 5 (2021) 96, https://doi.org/10.12688/gatesopenres.13233.3.